Modelling of combustion and knock onset risk in a high-performance turbulent jet ignition engine

Transportation Engineering 2 (2020) 100037

Contents lists available at ScienceDirect

Transportation Engineering

journal homepage: www.elsevier.com/locate/treng

Modelling of combustion and knock onset risk in a high-performance turbulent jet ignition engine

Andrea Bianco [a,*], Federico Millo [b], Andrea Piano [b]

[a] POWERTECH Engineering, Via Carolina Invernizio, 6, 10127 Torino, Italy
[b] Politecnico di Torino, Corso Duca degli Abruzzi, 24, 10129 Torino, Italy

ARTICLE INFO

Keywords:
Knock
Turbulent jet ignition
Internal combustion engine
3D-CFD combustion simulation
TJI

ABSTRACT

The reduction of CO_2 emissions, and hence of fuel consumption, is currently a key driver for the development of innovative SI engines for passenger car applications. In recent years, motorsport technical regulations in the highest categories have seen the introduction of limits concerning the fuel flow rate and the total amount of fuel per race, thus driving engine development toward further reduction of specific fuel consumption. Among the different techniques that can be shared between conventional and high-performance SI engines, turbocharging, compression ratio increase and Turbulent Jet Ignition (TJI) have shown a significant potential for fuel consumption reduction. The combination of turbocharging and compression ratio increase, however, can promote the onset of knocking combustion, with detrimental effects on engine's efficiency and durability. Additionally, engines equipped with TJI systems show unusual combustion development and knock onset.

In this study a methodology for the 3D-CFD modelling of combustion and knock onset risk was developed for a high-performance turbocharged engine featuring a passive TJI system. First, a comprehensive numerical study was carried out in a commercially available software, CONVERGE 2.4, in order to develop a 3D-CFD model able to reproduce the available experimental data. The resulting 3D-CFD model was then validated on different working conditions featuring different spark advances. Lastly, a methodology for the assessment of knock onset risk was developed, which led to the definition of two novel knock-risk indexes based on the progress of chemical reactions within the combustion chamber. The proposed knock-risk indexes showed good agreement with the experimental data.

1. Introduction

Due to the compelling need to decrease greenhouse gases emissions Governments all around the world are setting demanding targets on carbon dioxide (CO_2) emissions for the passenger car sector [1–3], thus driving the development of internal combustion engines toward further improvements in engine efficiency and fuel consumption reduction. As Spark Ignition (SI) engines nowadays account for 80% of the worldwide light duty powertrain mix [4] and are expected to remain the predominant technology in passenger car for decades to come [5], their improvement is mandatory to move towards more sustainable mobility. To this end, engine downsizing and turbocharging have been widely adopted in recent years by several car manufacturers, leading to significant improvement in specific fuel consumption [6].

The motorsport sector is facing similar trends after the technical revolution introduced in 2014 by the International Automotive Association (FIA) with the adoption of downsized SI engines in all major racing series, aiming at bringing motor-racing back to its role of extreme test bench for innovative technical solutions and increase technology transfer towards mass production vehicles. Additionally, major categories such as Formula One World Championship and World Endurance Championship have seen the introduction of limits concerning the fuel flow rate and the total amount of fuel per race, which coupled with stringent

Abbreviations: A/F, air-to-fuel ratio; ACTDC, after combustion top dead centre; AMR, adaptive mesh refinement; BMEP, brake mean effective pressure; BSFC, brake specific fuel consumption; CAD, crank angle degree; CCV, cycle-to-cycle variability; CFD, computational fluid dynamics; CFL, Courant–Friedrichs–Lewy; CO_2, carbon dioxide; CH_2O, formaldehyde; FIA, Federation International de l'Automobile; GDI, gasoline direct injection; IMEP, indicated mean effective pressure; KLSA, knock limited spark advance; LES, large eddy simulation; MAPO, maximum amplitude of pressure oscillations; MC, main chamber; MFB, mass of fuel burned; OH, hydroxide; PC, pre-chamber; RANS, Reynolds averaged Navier–Stokes; SI, spark ignition; ST, spark timing; TCI, turbulence–chemistry interaction; TDC, Top Dead Center; TJI, turbulent jet ignition; UDF, user defined function; WSR, well stirred reactors.

* Corresponding author.
E-mail address: a.bianco@pwt-eng.com (A. Bianco).

https://doi.org/10.1016/j.treng.2020.100037
Received 15 June 2020; Received in revised form 10 September 2020; Accepted 31 October 2020

technical regulations have driven engine development towards the path of specific fuel consumption reduction.

Among the different technologies available for both conventional powertrain and high-performance SI engines, downsizing coupled with turbocharging, compression ratio increase and Turbulent Jet Ignition (TJI) have shown a significant potential for fuel consumption reduction. The quest for continuously increasing engine efficiency faces however limitations in the usage of turbocharging and high compression ratios, due to the increase of knocking combustion likelihood, while a promising path is the adoption of lean Air-to-Fuel (A/F) operating conditions, for which TJI systems are a key enabler [7].

TJI systems can be classified in passive Pre-Chamber (PC) systems, in which the fuel is fed externally into the PC, and active PC systems, in which fuel is injected inside the PC, but only the former is currently adopted in modern motorsport engines because of regulations constraints. A passive PC consists of a cover with holes encapsulating a small volume of fluid and the spark plug electrodes, which is used as an enhancer of ignition energy for the Main combustion Chamber (MC): turbulent jets generated during PC combustion fill the MC of active radicals and create multiple ignition zones in the unburned mixture [7,8]. The energy transferred from PC to MC allows the adoption of higher A/F lean combustion limit and reduce MC combustion duration, enhancing thermal efficiency and reducing knock tendency [8,9] thus justifying the recent adoption of such technologies in motorsport engines.

Details concerning turbulent jet assisted combustion, however, are still to be fully understood due to the significant limitations in the experimental testing of pre-chambers, therefore TJI systems are still an open research field nowadays. Despite several studies, the knowledge on the detailed relations between PC jets and MC combustion process is still limited even if it could boost further improvement in engine efficiency by allowing a robust control of knocking and the adoption of innovative combustion techniques [10,11].

In this context, the advantage of performing 3D-CFD simulations is evident, as they could provide additional information which are not accessible through experiments. Recent studies using high-fidelity Large Eddy Simulations (LES) [12,13] have provided high level of details concerning TJI combustion development, but for the moment the LES methodology is considered unpractical in the context of motorsport and commercial engine development, as it demands enormous computational power such as thousands of cores and long simulation times [12]. Simulations based on Reynolds Averaged Navier–Stokes (RANS) equations are instead common practice in industrial environment, thanks to their relative simplicity and quick turnaround time, and have proven their reliability in the context of TJI modelling [14,15], thus having a remarkable potential for investigating jet ignition and combustion process, especially in the early stage of engine development. The availability of robust methodologies allowing the description of knock onset is however limited since RANS simulations are fundamentally bounded to the representation of the average engine cycle without accounting for Cycle-to-Cycle Variability (CCV). Given that CCV is significantly reduced in TJI engines ([9]) and hence knock onset is less dependant on chaotic perturbations of the average engine cycle, one of the possibilities to overcome the aforementioned limit is to correlate the average combustion development in end-gases for non-knocking conditions with the risk of autoignition, rather than modelling single knocking cycles. This would allow the definition of indexes that can be used in early engine design phases to gather useful information on knock likelihood and hence expected performance limits.

In this study a 3D-CFD methodology is presented for the modelling of TJI combustion and knock onset risk in a RANS framework, which was developed for a turbocharged racing engine under development featuring a passive PC. The purpose of the proposed methodology is the identification of new 3D-CFD indexes representing the risk of end-gases autoignition and abnormal combustion development, starting from the analysis of knock-free conditions. First, experimental tests were carried out in order to build a reliable database which was used as a reference in the modelling activity. Secondly, a comprehensive numerical study was carried out with the aim to develop a 3D-CFD model capable to reproduce the TJI combustion process, which has been previously experimentally characterized, and the resulting model was then validated on working conditions featuring different spark advances. Lastly, a methodology for the assessment of knock onset risk starting from the simulation of non-knocking conditions was developed, which led to the definition of two novel knock-risk indexes based on the progress of chemical reactions within the combustion chamber. The proposed knock-risk indexes were validated against available experimental data and showed good agreement.

Table 1
Test engine under study.

Parameter	Value
Cylinder displacement	~0.25 L
Bore / Stroke	~1.5
Compression ratio	>14:1
Turbocharger	Single-Stage
Fuel injection system	High-pressure GDI >400 bar
Combustion system	TJI w/ passive PC

Table 2
Engine working point.

Speed [rpm]	IMEP [bar]	Lambda [-]
12,500	>35	>>1

2. Methodology

2.1. Test engine and experimental data

The engine selected for the study is a high-performance 4-stroke SI prototype engine for motorsport applications, whose main characteristics are listed in Table 1. It features a single-stage turbocharging system and an extremely high compression ratio, characteristics that potentially boost thermal efficiency but increase both the risk of knock onset and abnormal combustion development. A wall-guided high-pressure Gasoline Direct Injection (GDI) system is used to allow the formation of an ignitable mixture in the passive PC during the compression stroke, using multiple injections and charge stratification strategies.

The analyses were performed for a single engine working point, which is listed in Table 2, representative of the most critical conditions in terms of delivered power and abnormal combustion risk, due to the lower flame velocity in lean mixtures

Experiments were carried out at engine manufacturer's facility using a special racing fuel (RON>102) that allowed the operation of the engine with a very high compression ratio, significantly higher than that of commercial SI engines in which it is typically limited by the knocking tendency of standard RON95 gasoline fuel. In-cylinder pressure traces in the Main Chamber (MC) were acquired with a resolution of 0.1 CAD for 200 consecutive engine cycles, using a piezo-electric transducer flush-mounted on one side of the combustion chamber. Additionally, pressure in intake and exhaust ports were recorded using high-speed sensors, while average temperature was acquired at intercooler outlet and exhaust manifold inlet. Three different experimental datasets were acquired in which spark timing was progressively advanced until knock-affected combustion was observed: they will be referenced as SA1, SA2 and SA3 in the following part of the study. In addition, a complete full-load performance curve was measured and used for validation purposes, as described in Section 2.2.

Finally, it is worth to be mentioned that the detailed chemical composition of the fuel was unknown both to the authors and to the engine

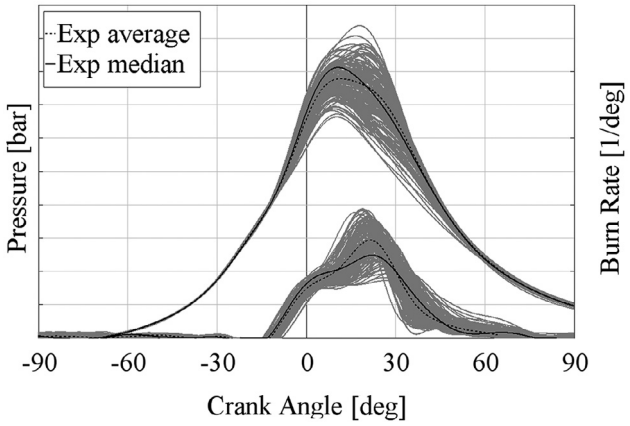

Fig. 1. Experimental MC pressure and calculated burn rate profiles at 12,500 rpm @ 100% load, SA3 spark advance, for ~200 consecutive non-knocking cycles (gray), average cycle (dashed black line) and median cycle (continuous black line).

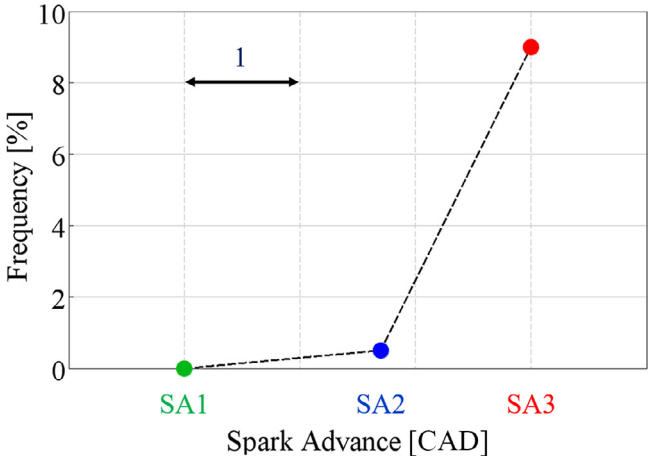

Fig. 2. Experimental frequency of knocking cycles at 12,500 rpm @ 100% load for different spark advances.

manufacturer, since fuel analysis is explicitly prohibited by motorsport technical regulations.

2.2. Analysis of experimental data

Post-processing of experimental data was carried out in GT-SUITE [16] by means of the 1D Three Pressure Analysis (TPA) methodology, which uses experimental intake and exhaust pressure data as input boundary conditions and calculates fuel burn rate from the measured in-cylinder pressure. For that purpose, a 3 kHz low pass-filter was applied on in-cylinder experimental pressure data for the calculation of average and median burn rate profiles. The TPA model was calibrated on the engine working point selected for the analysis and validated on a full load curve at different speeds. Predicted quantities such as average air flow rate, BMEP and BSFC showed good agreement with experimental data in each point of the full-load curve, with a maximum relative error lower than 5%. TPA results highlighted significant Cycle-to-Cycle Variability (CCV) in experimental data, as shown in Fig. 1.

The validated 1D model was then used for the generation of average boundary conditions for the 3D-CFD analysis.

TPA methodology was then used to extract information concerning knocking cycles. With this aim, in-cylinder pressure signals were band-pass filtered between 3 kHz and 20 kHz, allowing the description of the first 6 combustion chamber's resonant frequencies [17].

Finally, the Maximum Amplitude of Pressure Oscillations (MAPO) index was extracted from filtered pressure data and used to identify knocking cycles and knocking intensity. The statistical distribution of MAPO in experimental cycles moved from a Gaussian-like under knock-free operating conditions toward a skewed type for increasing spark advances, due to the increasing number of cycles showing knocking combustion and high-pressure oscillations at advanced spark timings (see Fig. 2 and [17] for more details). The resulting frequency of knocking cycles in each dataset changed significantly with spark advance, as summarized in Fig. 2, with a steep increase between SA2 and SA3 where a Knock Limited Spark Advance (KLSA) could be defined.

Lastly, analysis of burn rate profiles highlighted that combustion development was faster in knocking conditions. In particular the crank angle at which the Mass of Fuel Burned (MFB) reached 50% of the available fuel, referred as MFB50 in the following, was larger in knock-free conditions, while the combustion duration, summarized by the MFB10-90 crank angle, was significantly lower in knocking cycles. It can be concluded, therefore, that in the selected engine working point the knocking cycles are fast burning cycles and that combustion development prior of the knock-free MFB50 crank angle significantly influence end-gas autoignition. This information has been used in the following to assess the suitability of the 3D-CFD engine model.

2.3. 3D-CFD engine model

The 3D-CFD analyses presented in this paper were carried out by means of the CONVERGE CFD software v2.4.21 [18]. A comprehensive sensitivity analysis, which was not included for brevity, was carried out on different modelling parameters in order to build a reliable virtual representation of in-cylinder phenomena. The most significant model settings resulting from the analysis are summarized in Sections 2.3.1–2.3.4 while calibration and validation results are shown in Section 2.3.5.

2.3.1. Numerical setup

The numerical schemes considered in the study were a second-order central difference scheme for spatial discretization while a first order implicit Euler scheme was used for temporal discretization, with a variable time-step size satisfying the most stringent constraints among convection CFL (1), diffusion CFL (2) and Mach CFL (50). It is worth highlighting that the maximum CFL limit assumed for Mach number is not appropriate for an accurate simulation of knocking combustion, as pressure waves propagation would not be correctly described, but is rather sufficient for the description of autoignition onset. Since the objective of the study is the assessment of autoignition risk rather than the detailed description of knock-triggered pressure waves, the aforementioned settings were considered acceptable and resulted in significant computational time savings.

In addition, the maximum number of cells that a liquid parcel can travel in a single time-step was limited to 1.5 in order to assure an adequate resolution of spray development, which is mandatory to correctly describe mixture formation when stratification strategies are present. Finally, the Pressure Implicit with Splitting Operator (PISO) algorithm of Issa [19] was used for solving conservation equations, coupled with the Rhie-Chow scheme [20].

2.3.2. Mesh settings

A structured mesh is automatically generated by CONVERGE at runtime, using a proprietary cut-cell Cartesian grid generation methodology with a user defined base cell size. In the present work a basic grid size of 2 mm was chosen as a result of a grid sensitivity analysis, with several custom mesh refinements through which the local mesh size was reduced to a minimum of 0.125 mm. A specific refinement was used on PC holes which led to more than 15 cells per orifice length.

In addition, the Adaptive Mesh Refinement (AMR) algorithm was used to increase grid resolution only where the flow field is mostly

under-resolved, dynamically as the solution changes. AMR settings were optimized through a grid sensitivity analysis to obtain a good compromise between simulation running time and accuracy; for that purpose velocity and temperature sub-grid scales were set to 1 m/s and 2.5 K respectively and the minimum cell size was set to 0.125 mm.

The resulting maximum number of cells reached during the simulation was equal to 6 million and the simulation of a single cycle required 3 days on 72 Intel Xeon v4 cores.

2.3.3. Turbulence modelling

Turbulence modelling is of pivotal importance in the context of TJI modelling, especially when dealing with 3D-CFD simulations of engines running at extremely high revving speed. Not only turbulence development within MC and PC should be correctly described during intake and compression strokes, but the development of turbulent jets has to be correctly assessed since ignition and combustion within the cylinder are driven by turbulent mixing and chemistry [12]. As far as TJI systems are concerned, recent researches showed that the turbulent length scales inside PC and MC can vary significantly from less than one to few millimetres during the engine cycle, with wide spatial gradients [12,21], and this poses significant challenges to accurate turbulence modelling in a RANS framework. In this context recent researches showed that RANS simulations can still provide a good description of the various turbulent scales at least up to spark timing [14], while calibration of modelling constants could be required to correctly describe the MC combustion process because of the significant role of Turbulence-Chemistry Interaction (TCI) [12].

In this perspective, the RANS RNG k-ε turbulence model was used [22] as it was found to be robust and capable of account for flame-induced compression, expansion and rapid strain effects on the turbulent quantities. Preliminary 3D-CFD simulations showed MC ignition timing in good agreement with experimental data without the need of any modification of model constants, however specific calibration was required for the correct description of MC combustion development. This is justified in authors' opinion since the adopted combustion model does not account explicitly for TCI effects [18, see also Section 2.3.4] which could be particularly significant in the analysed engine working point because of the very high revving speed. A comprehensive sensitivity analysis performed on turbulent Prandtl and Schmidt numbers suggested that spatial variation of these nondimensional numbers would be the best option for the correct description of jet ignition, flame formation and propagation within the cylinder. However, the development of a model describing spatial variations of turbulent transport parameters was outside the scope of the study and the calibration of turbulent Prandtl and Schmidt numbers, linked to MC flame development, led to satisfactory results, therefore the latter approach was deemed sufficient for the present research.

Lastly, law-of-the-walls [23] were adopted for the description of kinetic and thermal boundary layers, with standard wall functions and adequate near-wall mesh settings. As far as the turbulent heat transfer modelling is concerned, among the different models available in CONVERGE the GruMo-UniMORE model [24] was used, as it was specifically developed for the description of heat transfer in turbocharged GDI SI engines.

2.3.4. Combustion modelling

In the 3D-CFD simulations framework, different combustion models have been used in recent researches to investigate TJI combustion, with encouraging results obtained using the Well-Stirred Reactor assumption (WSR) [13,25,26] as well as the flamelet assumption (ECFM [15,27] and G-equation [21]). Additional studies on TJI systems highlighted that multiple combustion regimes could be present within the cylinder, with MC combustion starting in a distributed reaction mode before switching to a flamelet propagation mode [12]. Adding lean combustion to the context could change significantly the combustion regimes observed during ignition and flame propagation as briefly summarized in Fig. 3.

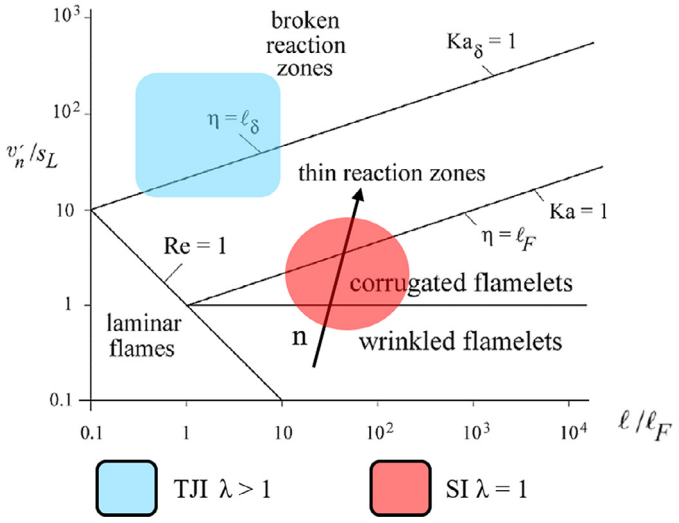

Fig. 3. Representation of expected combustion regimes on Borghi's diagram [29] for lean burn TJI engines (light blue area) and conventional homogeneous charge SI engines (red area). (For interpretation of the references to color in this figure legend, the reader is referred to the web version of this article.)

In particular, TJI system operated in lean conditions could be characterized by the broken reaction and thickened flames regimes rather than flamelets regimes [28]. Lastly, the high revving speed of the engine increases the thickness of reaction zones and could enhance the relevance of the broken reaction regime.

In this complex scenario the SAGE detailed chemistry combustion model [18], which is based on the WSR assumption, was selected for the study, as it is intrinsically capable to capture multiple volumetric ignition sites within the MC, differently than flamelet based models. With appropriate spatial resolutions the SAGE model allows broader applicability to combustion phenomena such as ignition and extinctions [30] and, in addition, it can be used for modelling both premixed and partially premixed combustion regimes, provided that accurate chemical reaction mechanism and fuel surrogate are used [31].

A comprehensive sensitivity study was performed to identify the most suitable fuel surrogate and reaction mechanism for the selected working point. The definition of a fuel surrogate without any detailed information concerning real fuel's composition was extremely challenging but, starting from literature methodologies [32], an appropriate 4-component fuel surrogate was identified by means of an extensive simulation campaign. The primary fuels included in the resulting fuel surrogate are toluene, n-heptane, isooctane and diisobutylene and their mass fractions (which cannot be disclosed for confidentiality reasons) were selected in order to match the fuel density, stoichiometric air/fuel ratio, lower heating value and RON. It is however worth highlighting that the presence of olefins such as diisobutylene was fundamental for the correct description of flame and end-gas interaction, as already confirmed by other studies [32]. As far as the chemical reaction mechanism is concerned, the extreme conditions of engine's operating point have forced compromise choices to be made. In more detail, to the authors' knowledge, none of the reaction schemes available in literature is validated for the extremely high pressure characterizing the selected engine working point. Therefore a reduced reaction mechanism from literature [33] was adopted (featuring 159 species and 734 reactions), since, on one hand, it was validated under conditions compatible with the thermodynamic state of in-cylinder gases at Top Dead Center (TDC) except for pressure, and on the other hand, it showed the best compromise between accuracy and simulation running time. Nevertheless, it was possible to obtain good results in the simulations without the need of any modification of the reaction scheme or combustion model parameters, which accord-

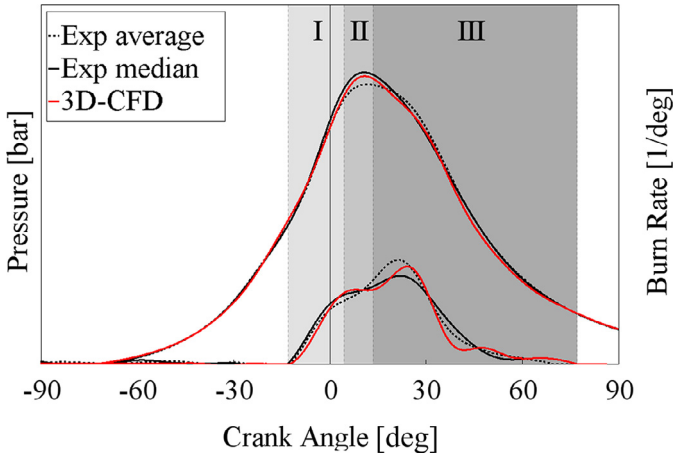

Fig. 4. Comparison of MC pressure and burn rate profiles between experimental average non-knocking cycle (dashed black line), median cycle (continuous black line) and 3D-CFD model results (red line) for spark advance SA3. The three phases of combustion are indicated with I, II and III. (For interpretation of the references to color in this figure legend, the reader is referred to the web version of this article.)

ing to the authors is a good indicator of robust calibration and realistic description of in-cylinder physics.

2.3.5. Results

Prior to the development of knock onset risk assessment methodology, the 3D-CFD model was calibrated and validated using the available experimental data. Since the purpose of the proposed methodology is the prediction of end-gas autoignition risk using 3D-CFD simulations of non-knocking cycles, calibration and validation were performed considering experimental datasets with the explicit exclusion of cycles showing abnormal combustion.

Fig. 4 shows a comparison of MC pressure and burn rate profiles between experimental dataset SA3 and results of the 3D-CFD model calibrated on the same engine operating condition. The experimental median cycle was extracted from pressure cycles ordered in ascending MAPO intensity and used for further comparisons. The calibration allowed a correct description of the start of combustion within the main chamber, as well as the initial development of the burn rate profile up to +6.5 CAD ACTDC. Visualization of this first stage of the combustion, labelled as I in Fig. 4, showed multiple ignition zones within the MC, with distributed reaction plumes departing from PC holes that can be ascribed as multiple well stirred reacting volumes. After +6.5 CAD ACTDC both the average and the median cycles shows a plateau in the MC burn rate profile, which lasts until +13.5 CAD ACTDC, and the 3D-CFD model correctly reproduce this event as well. This period of the engine cycle was identified as the second phase of MC combustion (II in Fig. 4) whose characteristic is the enlargement of distributed reaction zones until the fusion of reactive plumes and the formation of a single burning volume. The third stage of MC combustion development, marked as III in Fig. 4, starts with the formation of a single flame front propagating in the MC and shows a peak in the burn rate profiles around +22 CAD ACTDC, with different intensity between the average and the median cycles. The 3D-CFD model shows again the characteristic peak in the burn rate profile with an intensity closer to the average experimental cycle and a slight delay in timing, which was however considered acceptable. The three-stages combustion development in TJI systems has been observed experimentally in a recent research [9], giving further confirmation on the validity of the results reported in this study. As far as the MC pressure is concerned, data for the experimental median cycle and 3D-CFD model results are in very good agreement and peak in-cylinder pressure is reproduced with correct intensity and timing.

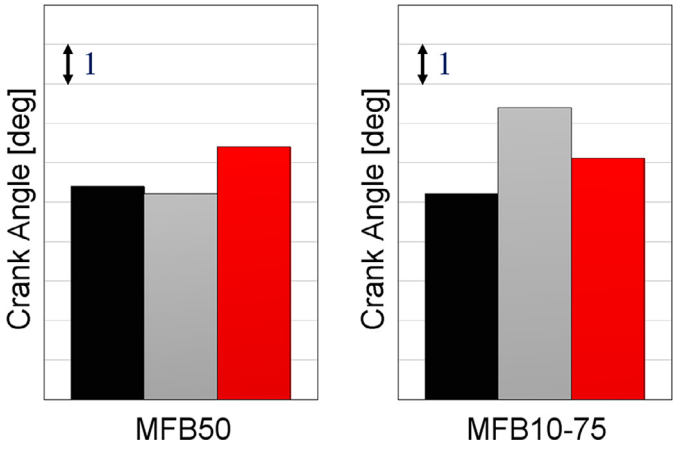

Fig. 5. Comparison of MC characteristic combustion angles MFB50 and MFB10–75 between experimental average non-knocking cycle (black), median cycle (grey) and 3D-CFD model results (red) for spark advance SA3. (For interpretation of the references to color in this figure legend, the reader is referred to the web version of this article.)

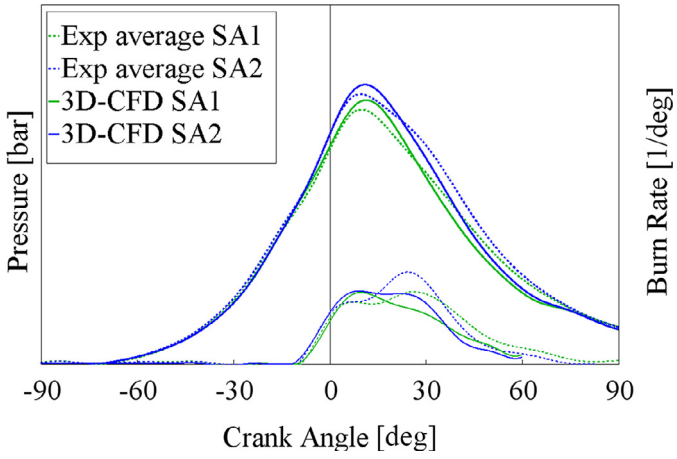

Fig. 6. Comparison of MC pressure and burn rate profiles between experimental average non-knocking cycles (dashed lines) and 3D-CFD model results (continuous lines) for spark advances SA1 and SA2. (For interpretation of the references to color in this figure legend, the reader is referred to the web version of this article.)

A comparison of MC characteristics combustion angles for the same conditions is also shown in Fig. 5. The agreement between experimental data and 3D-CFD results is very good, with differences in MFB50 below 1 CAD while the simulated combustion duration lays between that of average and median cycles.

Validation of the 3D-CFD model was performed through a spark timing sweep, consistently with experiments. MC pressures and burn rate profiles resulting from the validation process are shown in Fig. 6 for spark advance SA1 and SA2. The agreement between experimental data and 3D-CFD results is more than satisfactory in the first stage of MC combustion development, up to +5/+6 CAD ACTDC, therefore the multiple ignitions of in-cylinder unburned mixture are expected to be correctly described in the simulations. After these crank angles, some differences arise in the second phase of MC combustion between simulation and experiments, probably because the turbulent interaction between adjacent reactive plumes is only partially described in the 3D-CFD models, due to lacking TCI effects. However, it is worth highlighting that experiments at different spark timings show a similar plateau in burn rate profiles during this second stage, and 3D-CFD results show an identical behaviour with only a slight shift in intensity. The third phase of the

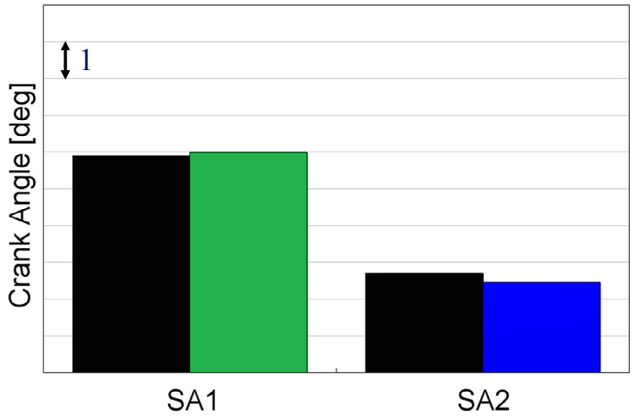

Fig. 7. Comparison of MC MFB50 crank angle between experimental non-knocking cycles (black) and 3D-CFD model results (green/blue) for spark advance SA1 and SA2. (For interpretation of the references to color in this figure legend, the reader is referred to the web version of this article.)

combustion, starting around +15 CAD ATDC, is the one showing larger differences between simulation results and experimental data and this could be attributed to the possible transition from a WSR combustion regime to a thick flame or flamelet regime, as recently found in other researches [12]. Since the SAGE combustion model adopted in the study is based on the WSR assumption, it is expected that some approximations could be observed in the description of a propagating flame, especially if TCI effects are significant. As far as the overall comparison is concerned it is important to note that experimental data show an increase in burn rate peak when moving from SA1 to SA2 and this trend is qualitatively reproduced by the 3D-CFD model as well.

Lastly, a comparison of MFB50 crank angle between experimental data and 3D-CFD results is shown in Fig. 7 and highlights that a very good agreement was achieved in the description of MC reactions progress, with deviations lower than 1 CAD. Since experimental data have shown that the initial combustion development is a key driver influencing the autoignition of end-gases and that the 3D-CFD model is able to correctly reproduce MC combustion at least up to the MFB50 crank angle, the agreement between simulation results and experiments was deemed sufficient for the development of the knock risk assessment methodology.

2.4. Knock onset risk assessment methodology

One of the advantages of the 3D-CFD model settings adopted in this study is the availability of a combustion model reliant on detailed chemistry, which allows the definition of risk indexes based on the progress of chemical reactions. According to the autoignition theory of knocking combustion [34], the fuel-air mixture in end-gases which is compressed to sufficiently high pressures and temperatures undergoes preflame reactions that can end up in rapid energy release and spontaneous autoignition. The chemical mechanism bringing to autoignition consists of a large number of simultaneous exothermal reactions in which highly reactive radicals are produced, then chain-branching reactions increase the number of radicals until a critical concentration or temperature is reached and autoignition is observed. Following this phenomenology, it is possible to assess the progress of preflame reactions provided that a suitable chemical species is identified, which should be representative of the complex chain-branching and degenerate-branching mechanisms. In this study formaldehyde (CH_2O) has been selected as the most appropriate chemical species representing the progress of preflame reactions, the choice being supported by several researches in which formaldehyde was found to provide quantitative evidence of temperature and reactions progress in end-gases [35-37]. Lastly, there are experimental evidences showing significant formaldehyde formation in end-gases just before autoignition [38-40].

In order to verify the suitability of the selected reaction mechanism for the description of formaldehyde formation in end-gases, a careful analysis of the reaction scheme was performed, which showed that CH_2O can be created independently from any of the four fuel surrogate's components and therefore the influence of fuel composition on end-gas reactivity is formally considered in the model. Additionally, several virtual sensors were placed close to the cylinder liner and used to gather information concerning the evolution of low temperature reactions in the simulation of knock free engine cycles, which were extracted from SA3 spark advance operating conditions. Fig. 8 shows twelve virtual sensors positioned in end-gases and the corresponding evolution of sampled chemical species in one specific sensor (#8), giving results consistent with the expected phenomenology. More in specific, Fig. 8(b) shows that formaldehyde is progressively created during the engine cycle and then suddenly disappears as soon as combustion starts, which is indicated by a steep increase in local OH concentration and gas temperature. It should be highlighted that the sudden decrease in CH_2O concentration does not provide any information concerning the nature of combustion, namely if it consists in autoignition or is due to flame propagation, but rather is only an indication of combustion timing. Since simulations showed that the progress of preflame reactions is proportional to formaldehyde formation, in the present study the mass fraction of CH_2O was assumed as an indicator of low temperature reaction progress and hence autoignition risk.

Two knock risk indexes were hence defined:

1. A global knock risk index represented by the overall CH_2O mass within the MC.
2. A local knock risk index represented by the unburned mass fraction reaching a critical CH_2O concentration.

Fig. 9 shows the local formaldehyde concentration for twelve sensors placed in the MC and highlights that three specific sensors, namely #4, #5 and #6, have recorded higher maximum mass fractions than the others and hence have identified the zone of the combustion chamber most prone to knock onset. Additionally, sensor #5 and #6 show a peak in CH_2O concentration around +23 CAD ACTDC, earlier than sensor #4 which shows a peak at +26.5 CAD ACTDC. Information concerning CH_2O peak intensities and timings translates in different risks of autoignition: preflame reactions are most-likely completed in sensor #5 and #6 and only later in sensor #4, therefore the gas zone entrained between sensors #5 and #6 is the most critical from the knock perspective.

In order to define a local autoignition risk index a CH_2O critical mass fraction was defined, indicated as "Γ" in Fig. 9(b), and was associated with the maximum risk of knock onset. Twenty bins were then defined having increasing mass fractions of formaldehyde, each one associated to an increasing knock onset risk. This classification was then used to monitor the evolution of in-cylinder unburned gases during the engine cycle and finally assess the risk of autoignition.

3. Results and discussion

Validation of the proposed knock risk indexes was performed against experimental data for different spark advances. The extraction of information concerning CH_2O development was implemented in a User Defined Function (UDF) which was linked to the 3D-CFD software, and simulations of knock-free cycles were run again without any setup modification.

As far as the global knock risk index is concerned, Fig. 10 shows the evolution of the overall formaldehyde mass within MC for different spark advances and highlights a qualitative agreement with experimental data of Fig. 2. There are, however, significant differences between the rate of increase with advancing spark advance of CH_2O mass in the

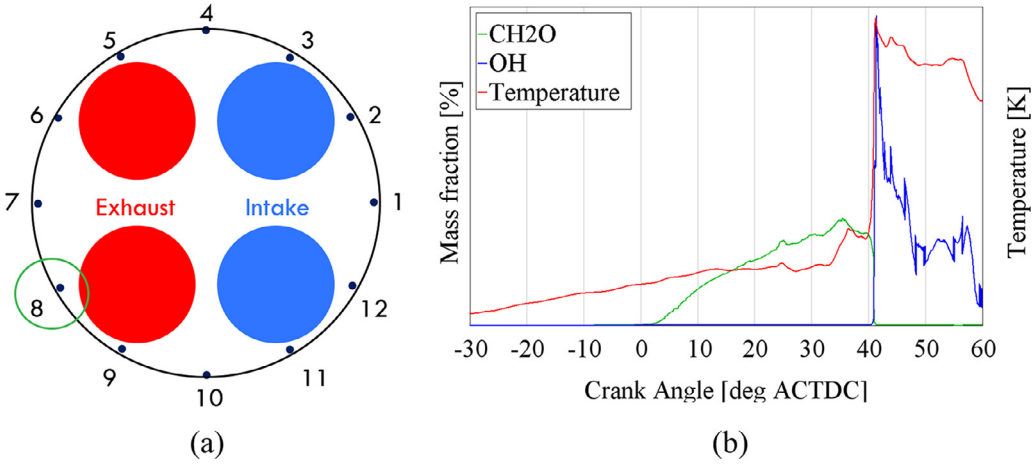

Fig. 8. (a) Overview of MC virtual sensors positioned near cylinder liner in the 3D-CFD engine model. (b) Mass fraction of CH2O (green), OH (blue) and gas temperature (red) measured in sensor #8 during the simulation of knock-free conditions, SA3 spark advance. (For interpretation of the references to color in this figure legend, the reader is referred to the web version of this article.)

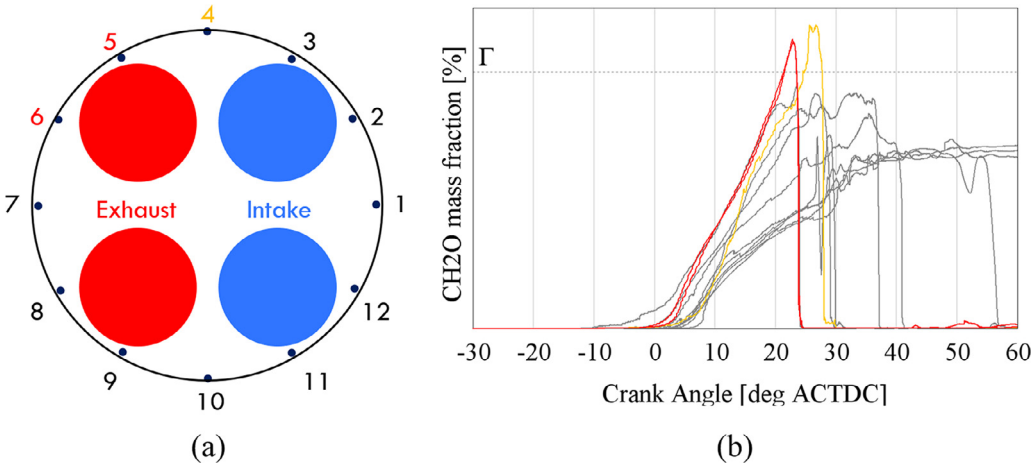

Fig. 9. (a) Overview of MC virtual sensors and (b) corresponding CH_2O local mass fraction during the simulation of knock-free conditions, SA3 spark advance. Signals from sensor #5 and #6 are shown in red while signal from sensor #4 is shown in orange and other sensors' signals are shown in grey. (For interpretation of the references to color in this figure legend, the reader is referred to the web version of this article.)

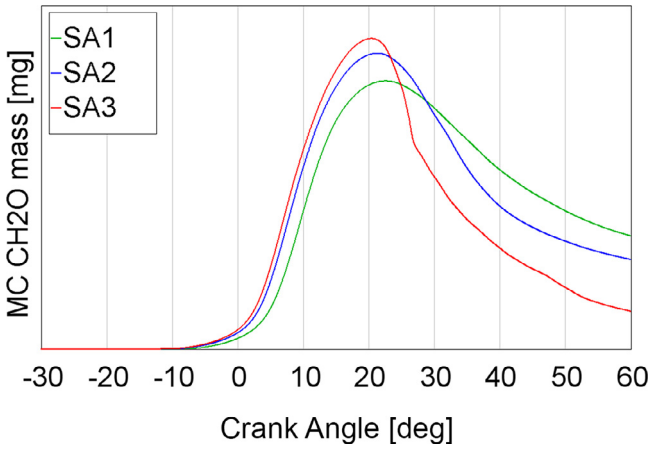

Fig. 10. Evolution of MC overall CH_2O mass from 3D-CFD simulations of different spark advances: SA1 (green), SA2 (blue) and SA3 (red). (For interpretation of the references to color in this figure legend, the reader is referred to the web version of this article.)

MC and that of knocking cycles frequency, the former being almost linear while the latter being exponential. For this reason, even though the global knock risk index shows qualitative agreement with experimental data, it is not further analysed in the rest of the study.

As far as the local knock risk index is concerned, Fig. 11 shows results obtained from 3D-CFD simulations of non-knocking cycles for the three different spark advances. The colored islands in Fig. 11 show the development of preflame reactions in MC unburned mixture and allow the assessment of autoignition risk; the left side of each coloured island represents the speed at which the pre-ignition reactions advance during the engine cycle toward the critical CH_2O bin #20, while the colour scale represents the amount of in-cylinder unburned mass in which these reactions occur. Similar features can be identified in Fig. 11 for different spark advances, in particular two red bands can be noticed between TDC and +15 CAD ACTDC which are representative of distinct effects due to flame propagation and end-gases reactions. At each crank angle the heat transfer from the flame causes a significant formation of CH_2O in the unburned gases next to the reacting front, while the flame propagation simultaneously consumes the formaldehyde previously created in the reaction zone. CH_2O concentration in unburned gases next to the flame front is therefore limited by the two competing processes and this is represented in Fig. 11 by the red band having lower bin num-

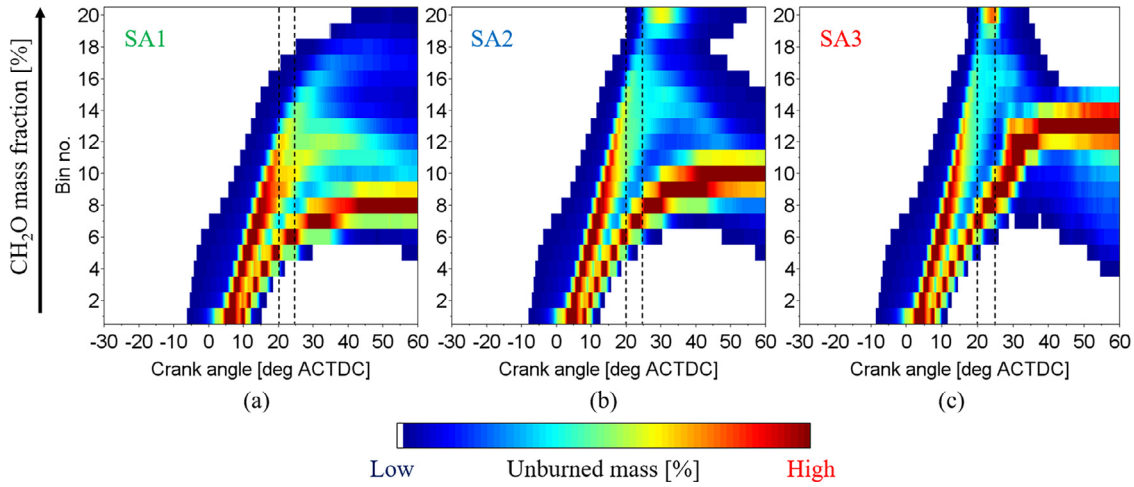

Fig. 11. 3D-CFD evolution of unburned mass fraction in CH_2O bins for non-knocking cycles at difference spark advances: SA1 (a), SA2 (b) and SA3 (c).

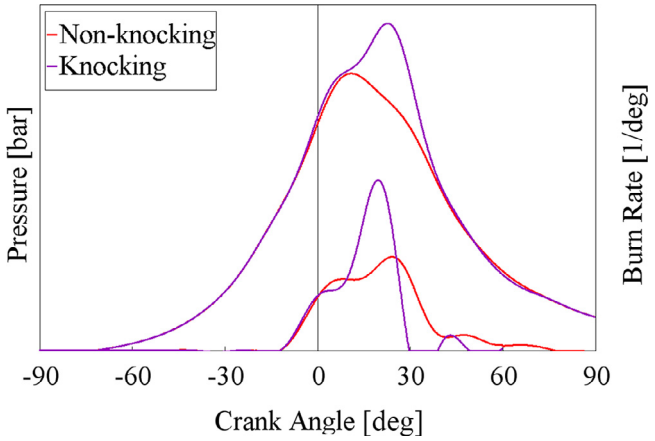

Fig. 12. Comparison of 3D-CFD MC pressure and burn rate profiles between non-knocking (red) and knocking (purple) cycles for spark advance SA3. (For interpretation of the references to color in this figure legend, the reader is referred to the web version of this article.)

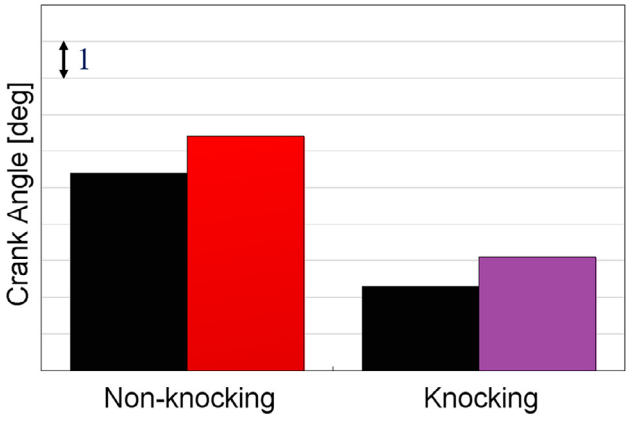

Fig. 13. Comparison of MC characteristic combustion angle MFB50 between experimental data (black) and 3D-CFD results for non-knocking (red) and knocking (purple) conditions at spark advance SA3. (For interpretation of the references to color in this figure legend, the reader is referred to the web version of this article.)

bers. At the same time pre-flame reactions in unburned gases which are not in direct contact with the flame cause a significant increase of local formaldehyde concentration. In this case CH_2O is not consumed until the flame reaches the end-gases or autoignition starts locally, therefore the resulting red band develops towards higher bin numbers. As far as the end-gases are concerned, Fig. 11 shows significant differences in the development of preflame reactions for different spark timings. Simulation results for spark advance SA1 show negligible unburned mass reaching bin #20 and, in addition, only after +40 CAD ACTDC, when MC combustion is almost completed, therefore representing a low risk of knock onset according to the model. Data concerning spark advance SA2 on the contrary show a moderate fraction of unburned gases reaching bin #20, starting from +20 CAD ACTDC, with a maximum concentration around +30 CAD ACTDC. This increased mass of unburned gases reaching the critical concentration of formaldehyde is representative of an increased risk of autoignition, compared to spark advance SA1. Lastly, moving to spark advance SA3, simulation results show the highest fraction of unburned gases reaching bin #20, starting already at +15 CAD ACTDC. Moreover, the rate of increase of unburned mass fraction in bin #20 is the highest among the different cases, as shown by the colors turning rapidly from blue to dark red in less than 5 CAD. Both the absolute value and the growth rate of unburned mass fraction in bin #20 are indicative of significant increase in knock onset risk for spark advance SA3 compared to previous cases, an outcome that is in very good agreement with the experimental results of Fig. 2. Not only the proposed methodology is able to predict the increased knock onset risk of spark advance SA3, but also the exponential growth of experimental knocking frequency is well represented in 3D-CFD results by the increasing fraction of unburned gases in bin #20 and its temporal evolution.

Since the proposed local knock index can provide information concerning the possible localization of autoignition spots within the combustion chamber, an additional simulation was eventually performed in knocking conditions to assess the validity of the forecasts. A fast-burning cycle having spark timing SA3 was simulated in 3D-CFD by artificially triggering faster combustion development through TCI effects and hence modification of turbulent Prandtl and Schmidt numbers. A comparison of the results obtained in non-knocking and knocking conditions for spark advance SA3 is shown in Figs. 12 and 13, the latter showing a very good agreement between experimental and predicted MFB50 crank angle in knocking conditions.

Information concerning the development of preflame reaction in knocking conditions are shown in Fig. 14 and differ significantly compared to non-knocking cycles: the unburned mass reaching bin #20 is the maximum observed among all the simulations and its growth rate is extremely high, varying from low to high concentrations in 2 CAD (17 CAD ACTD to 19 CAD ACTDC). Moreover, looking at the right side of the

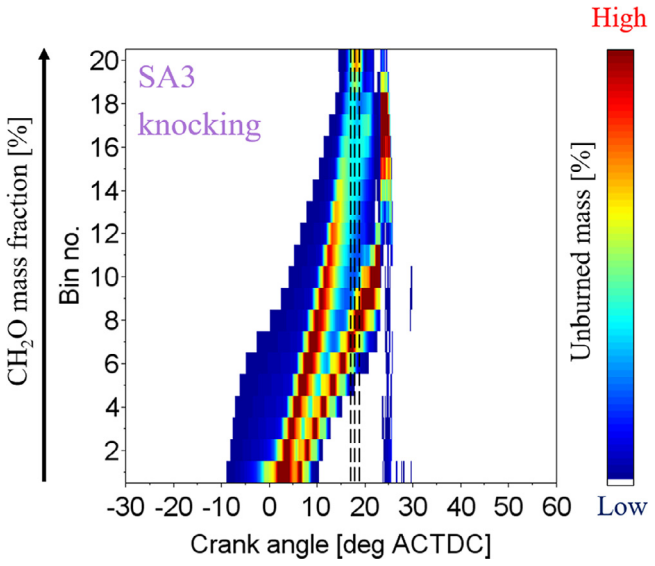

Fig. 14. 3D-CFD evolution of unburned mass fraction in CH_2O bins for a knocking cycle at spark advance SA3.

coloured island it can be noticed a sudden disappearance of unburned mass fraction in all formaldehyde bins at roughly +25 CAD ACTDC, which is representative of an extremely fast generalized combustion following the appearance of knock onset. Fig. 15 shows a contour plot of formaldehyde distribution in end gases during the crank angle period previously identified and can be used to identify the knock onset position. The flame front highlighted in Fig. 15(a) moves significantly ahead between sensor #5 and #6 in just 1 CAD, as shown in Fig. 15(b), indicating knock onset in the exact position predicted by the analysis of non-knocking cycles. In addition, the developing flame front moves preferentially towards sensor #4 at +19 CAD ACTDC, Fig. 15(c), which is again in good agreement with the forecast of the proposed model. The information shown highlights, therefore, the good agreement of the proposed local knock risk index with the actual development of self-combustion both in terms of occurrence and positioning.

4. Conclusions

In this paper a 3D-CFD RANS methodology for the modelling of combustion development in TJI systems and the assessment of knock onset risk was presented.

Starting from experimental data acquired on a high-performance TJI engine prototype, a 3D-CFD RANS model was developed, calibrated, and used to investigate in-cylinder combustion development, showing peculiar characteristics in burn rate profiles linked to PC jets interaction. Specific calibration was performed to account for turbulence and TCI effects, the role of which was found to be not negligible at very lean A/F ratios. The 3D-CFD model was validated against experimental data and showed the ability to correctly describe the main features of the combustion process, even if some limitations still arise which can be attributed to the necessity to account for multiple combustion regimes in a single simulation.

After that, a new methodology, based on detailed chemistry simulation of the combustion process, was proposed for the assessment of knock onset risk starting from the 3D-CFD analysis of non-knocking cycles. Two new knock risk indexes were proposed:

1. A global knock risk index, represented by the overall mass of formaldehyde within the MC. The index showed qualitative agreement with experimental data but was not able to reproduce the exponential growth of knocking cycles frequency for different spark advances.
2. A local knock risk index, represented by the unburned mass fraction reaching a critical concentration of formaldehyde inside the MC. The index showed a very good agreement with experimental data as it allowed the correct assessment of knock onset risk from the analysis of knock-free cycles. In addition, the index was used to identify critical zones of the combustion chamber that are prone to knock and showed very good agreement with the results of a simulation reproducing knocking conditions.

Lastly, since there are experimental evidences showing significant formaldehyde formation in end-gases just before autoignition, the proposed methodology has the potential to be validated through specific tests on optical accessible engines.

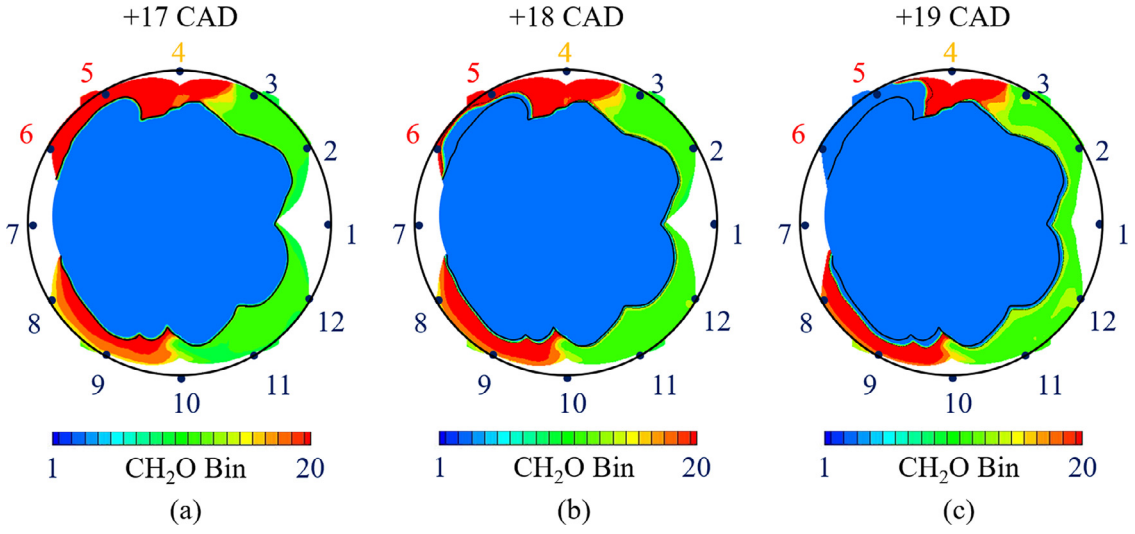

Fig. 15. Contour plot of formaldehyde concentration in MC end-gases at 3 specific crank angles in knocking conditions: incipient knock (a), autoignition started (b), reaction propagation (c). SA3 spark advance. The black line highlights flame position at +17 CAD ACTDC.

Declaration of Competing Interest

The authors declare that they have no known competing financial interests or personal relationships that could have appeared to influence the work reported in this paper.

Acknowledgements

Computational resources were provided by HPC@POLITO (http://www.hpc.polito.it).

References

[1] Regulation (EU) 2019/631 of the European Parliament and of the Council of 17 April 2019 setting CO2 emission performance standards for new passenger cars and for new light commercial vehicles, and repealing regulations (EC) no 443/2009 and (EU) no 510/2011. 2019. Available from: http://data.europa.eu/eli/reg/2019/631/oj (Accessed on 10/06/2020).
[2] The Safer Affordable Fuel Efficient (SAFE) Vehicles final rule for model years 2021-2026, United States Environmental Protection Agency (EPA), 40 CFR parts 86 and 600. 2020. Available from: https://www.govinfo.gov/content/pkg/FR-2020-04-30/pdf/2020-06967.pdf (Accessed on 10/06/2020).
[3] Continental, Worldwide emission standards and related regulations, passenger cars/light and medium duty vehicles, 2019.
[4] OPEC, World oil outlook 2019. Available from: https://woo.opec.org/ (Accessed on 10/06/2020).
[5] F. Leach, G. Kalghatgi, R. Stone, P. Miles, The scope for improving the efficiency and environmental impact of internal combustion engines, Transp. Eng. 1 (2020), doi:10.1016/j.treng.2020.100005.
[6] The International Council on Clean Transportations - ICCT, European vehicle market statistics – pocketbook 2019/2020. 2020, Available from: http://eupocketbook.org/ (Accessed on 10/06/2020).
[7] C.E. Castilla Alvarez, G. Elias Couto, V. Ruckert Roso, A. Braga Thiriet, R. Molina Valle, A review of prechamber ignition systems as lean combustion technology for SI engines, Appl. Therm. Eng. 128 (2018) 107–120, doi:10.1016/j.applthermaleng.2017.08.118.
[8] W.P. Attard, N. Fraser, P. Parsons, E. Toulson, A turbulent jet ignition pre-chamber combustion system for large fuel economy improvements in a modern vehicle powertrain, SAE Tech. Pap. (2010), doi:10.4271/2010-01-1457.
[9] J. Hua, L. Zhou, Q. Gao, Z. Feng, H. Wei, Effects on cycle-to-cycle variations and knocking combustion of turbulent jet ignition (TJI) with a small volume prechamber, SAE Tech. Pap. (2020), doi:10.4271/2020-01-1119.
[10] W.P. Attard, H. Blaxill, E.K. Anderson, P. Litke, Knock limit extension with a gasoline fuelled pre-chamber jet igniter in a modern vehicle powertrain, SAE Tech. Pap. (2012), doi:10.4271/2012-01-1143.
[11] D. Koch, V. Berger, A. Bittel, M. Gschwandtner, et al., Investigation of an innovative combustion process for high-performance engines and its impact on emissions, SAE Tech. Pap. (2019), doi:10.4271/2019-01-0039.
[12] Q. Malé, G. Staffelbach, O. Vermorel, A. Misdariis, F. Ravet, et al., Large eddy simulation of pre-chamber ignition in an internal combustion engine, Flow, Turbulence and Combustion, Springer Verlag, Germany, 2020 in press, doi:10.1007/s10494-019-00026-y.
[13] M. Muller, C. Freeman, P. Zhao, H. Ge, Numerical simulation of ignition mechanism in the main chamber of turbulent jet ignition system, in: Proceedings of the ASME Internal Combustion Engine Division Fall Technical Conference, 2, ASME, 2018, doi:10.1115/ICEF2018-9587.
[14] M. Bolla, E. Shapiro, N. Tiney, P. Kyrtatos, et al., Numerical study of turbulence and fuel-air mixing within a scavenged pre-chamber using RANS and LES, SAE Tech. Pap. (2019), doi:10.4271/2019-01-0198.
[15] R. Novella, J. Pastor, J. Gomez-Soriano, I. Barbery, et al., Experimental and numerical analysis of passive pre-chamber ignition with EGR and air dilution for future generation passenger car engines, SAE Tech. Pap. (2020), doi:10.4271/2020-01-0238.
[16] GTSUITE Engine Performance Application Manual, Gamma Technologies, 2016.
[17] F. Millo, C. Ferraro, Knock in S.I. engines: a comparison between different techniques for detection and control, SAE Tech. Pap. (1998), doi:10.4271/982477.
[18] K.J. Richards, P.K. Senecal, E. Pomraning, CONVERGE 2.4 Manual, Convergent Science, Madison, WI, 2019.
[19] R.I. Issa, Solution of the implicitly discretised fluid flow equations by operator-splitting, J. Comput. Phys. 62 (1) (1986) 40–65, doi:10.1016/0021-9991(86)90099-9.
[20] C.M. Rhie, W.L. Chow, Numerical study of the turbulent flow past an airfoil with trailing edge separation, AIAA J. 21 (11) (1983) 1525–1532, doi:10.2514/3.8284.
[21] G. Xu, Y.M. Wright, M. Schiliro, K. Boulouchos, Characterization of combustion in a gas engine ignited using a small un-scavenged pre-chamber, Int. J. Engine Res. (2018), doi:10.1177/1468087418798918.
[22] V. Yakhot, S.A. Orszag, S. Thangam, T.B. Gatski, C.G. Speziale, Development of turbulence models for shear flows by a double expansion technique, Phys. Fluids A (1992), doi:10.1063/1.858424.
[23] H.K. Versteeg, W. Malalasekera, An Introduction to Computational Fluid Dynamics: The Finite Volume Method, 2nd edition, Pearson Education Limited, 2007 ISBN: 978-0-13-127498-3.
[24] F. Berni, G. Cicalese, S. Fontanesi, A modified thermal wall function for the estimation of gas-to-wall heat fluxes in CFD in-cylinder simulations of high performance spark-ignition engines, Appl. Therm. Eng. 115 (2017) 1045–1062, doi:10.1016/j.applthermaleng.2017.01.055.
[25] M.E. Feyz, et al., Large eddy simulation of hot jet ignition in moderate and high-reactivity mixtures, Comput. Fluids 183 (2019) 28–37.
[26] M. Gholamisheeri, B. Thelen, G. Gentz, E. Toulson, CFD modeling of an auxiliary fuelled turbulent jet ignition system in a rapid compression machine, SAE Tech. Pap. (2016), doi:10.4271/2016-01-0599.
[27] O. Laget, S. Chevillard, G. Pilla, X. Gautrot, et al., Investigations on pre-chamber ignition device using experimental and numerical approaches, SAE Tech. Pap. (2019), doi:10.4271/2019-01-2163.
[28] R. Scarcelli, N. Matthias, T. Wallner, Numerical investigation of combustion in a lean burn gasoline engine, SAE Tech. Pap. (2013), doi:10.4271/2013-24-0029.
[29] R. Borghi, M. Destriau, Combustion and Flames, Chemical and Physical Principles, Editions Technip, Paris, 1998.
[30] P.K. Senecal, K. Richards, E. Pomraning, T. Yang, et al., A new parallel cut-cell Cartesian CFD code for rapid grid generation applied to in-cylinder diesel engine simulations, SAE Tech. Pap. (2007), doi:10.4271/2007-01-0159.
[31] M.E. Feyz, “Analytical and Computational Study of Turbulent-Hot Jet Ignition Process in Methane-Hydrogen-Air Mixtures”, Purdue University Graduate School, PhD Thesis. doi:10.25394/PGS.11336915.v1.
[32] P. Ghosh, K.J. Hickey, S.B. Jaffe, Development of a detailed gasoline composition-based octane model, Ind. Eng. Chem. Res. 45 (1) (2006) 337–345, doi:10.1021/ie050811h.
[33] J.C.G. Andrae, T. Kovàcs, Evaluation of adding an olefin to mixtures of primary reference fuels and toluene to model the oxidation of a fully blended gasoline, Energy Fuels 30 (9) (2016) 7721–7730, doi:10.1021/acs.energyfuels.6b01193.
[34] J.B. Heywood, Internal Combustion Engine Fundamentals, McGraw-Hill, New York, 1988.
[35] H. Zhao, HCCI and CAI Engines for the Automotive Industry, Woodhead Publishing, 2007 ISBN 9781845691288.
[36] Z. Wang, H. Liu, R.D. Reitz, Knocking combustion in spark-ignition engines, Prog. Energy. Combust. Sci. 61 (2017) 78–112 ISSN 0360-1285, doi:10.1016/j.pecs.2017.03.004.
[37] Z. Wang, Y. Wang, R.D. Reitz, Pressure oscillation and chemical kinetics coupling during knock processes in gasoline engine combustion, Energy Fuels 26 (2012) 7107–7119.
[38] J. Wanatz, U. Maas, R. Dibble, Combustion: Physical and Chemical Fundamentals, Modeling and Simulation, Experiments, Pollutant Formation, Springer, 2006, doi:10.1007/978-3-540-45363-5.
[39] R. Suzuki, H. Shoji, K. Yoshida, A. Iijima, Analysis of knocking in an SI engine based on in-cylinder: spectroscopic measurements and visualization, SAE Tech. Pap. (2010), doi:10.4271/2010-32-0092.
[40] R. Schiebl, U. Maas, Analysis of endgas temperature fluctuations in an SI engine by laser-induced fluorescence, Combust. Flame 133 (2003) 19–27.